Nuclear Inst. and Methods in Physics Research, A 1040 (2022) 167132

Contents lists available at ScienceDirect

Nuclear Inst. and Methods in Physics Research, A

journal homepage: www.elsevier.com/locate/nima

Nanobeacon: A time calibration device for the KM3NeT neutrino telescope

S. Aiello [1], A. Albert [53,2], M. Alshamsi [3], S. Alves Garre [4], Z. Aly [5], A. Ambrosone [6,7], F. Ameli [8], M. Andre [9], G. Androulakis [10,a], M. Anghinolfi [11], M. Anguita [12], M. Ardid [13], S. Ardid [13], J. Aublin [3], C. Bagatelas [10], B. Baret [3], S. Basegmez du Pree [14], M. Bendahman [3,15], F. Benfenati [16,17], E. Berbee [14], A.M. van den Berg [18], V. Bertin [5], S. Biagi [19], M. Boettcher [20], M. Bou Cabo [21], J. Boumaaza [15], M. Bouta [22], M. Bouwhuis [14], C. Bozza [23], H. Brânzaş [24], R. Bruijn [14,25], J. Brunner [5], R. Bruno [1], E. Buis [26], R. Buompane [6,27], J. Busto [5], B. Caiffi [11], D. Calvo [4], S. Campion [28,8], A. Capone [28,8], V. Carretero [4], P. Castaldi [16,29], S. Celli [28,8], M. Chabab [30], N. Chau [3], A. Chen [31], S. Cherubini [19,32], V. Chiarella [33], T. Chiarusi [16], M. Circella [34], R. Cocimano [19], J.A.B. Coelho [3], A. Coleiro [3], M. Colomer Molla [3,4], R. Coniglione [19], P. Coyle [5], A. Creusot [3], A. Cruz [35], G. Cuttone [19], R. Dallier [36], B. De Martino [5], I. Di Palma [28,8], A.F. Díaz [12], D. Diego-Tortosa [13], C. Distefano [19], A. Domi [14,25], C. Donzaud [3], D. Dornic [5], M. Dörr [37], D. Drouhin [53,2], T. Eberl [38], A. Eddyamoui [15], T. van Eeden [14], D. van Eijk [14], I. El Bojaddaini [22], S. El Hedri [3], A. Enzenhöfer [5], V. Espinosa [13], P. Fermani [28,8], G. Ferrara [19,32], M.D. Filipović [39], F. Filippini [16,17], L.A. Fusco [5], T. Gal [38], J. García Méndez [13], F. Garufi [6,7], Y. Gatelet [3], C. Gatius Oliver [14], N. Geißelbrecht [38], L. Gialanella [6,27], E. Giorgio [19], S.R. Gozzini [4], R. Gracia [14], K. Graf [38], G. Grella [40], D. Guderian [54], C. Guidi [11,41], B. Guillon [42], M. Gutiérrez [43], J. Haefner [38], S. Hallmann [38], H. Hamdaoui [15], H. van Haren [44], A. Heijboer [14], A. Hekalo [37], L. Hennig [38], J.J. Hernández-Rey [4], J. Hofestädt [38], F. Huang [5], W. Idrissi Ibnsalih [6,27], G. Illuminati [16,3,17], C.W. James [35], D. Janezashvili [45], M. de Jong [14,46], P. de Jong [14,25], B.J. Jung [14], P. Kalaczyński [47], O. Kalekin [38], U.F. Katz [38], N.R. Khan Chowdhury [4], G. Kistauri [45], F. van der Knaap [26], P. Kooijman [25,55], A. Kouchner [3,48], V. Kulikovskiy [11], M. Labalme [42], R. Lahmann [38], M. Lamoureux [3,b], G. Larosa [19], C. Lastoria [5], A. Lazo [4], R. Le Breton [3], S. Le Stum [5], G. Lehaut [42], O. Leonardi [19], F. Leone [19,32], E. Leonora [1], N. Lessing [38], G. Levi [16,17], M. Lincetto [5], M. Lindsey Clark [3], T. Lipreau [36], C. LLorens Alvarez [13], F. Longhitano [1], D. Lopez-Coto [43], L. Maderer [3], J. Majumdar [14], J. Mańczak [4], A. Margiotta [16,17], A. Marinelli [6], C. Markou [10], L. Martin [36], J.A. Martínez-Mora [13], A. Martini [33], F. Marzaioli [6,27], S. Mastroianni [6], K.W. Melis [14], G. Miele [6,7], P. Migliozzi [6], E. Migneco [19], P. Mijakowski [47], L.S. Miranda [49], C.M. Mollo [6], M. Moser [38], A. Moussa [22], R. Muller [14], M. Musumeci [19], L. Nauta [14], S. Navas [43], C.A. Nicolau [8], B. Nkosi [31], B. Ó Fearraigh [14,25], M. O'Sullivan [35], M. Organokov [2], A. Orlando [19], J. Palacios González [4], G. Papalashvili [45], R. Papaleo [19], A.M. Păun [24], G.E. Păvălaş [24], C. Pellegrino [17,56], M. Perrin-Terrin [5], V. Pestel [14], P. Piattelli [19], C. Pieterse [4], O. Pisanti [6,7], C. Poirè [13], V. Popa [24], T. Pradier [2], I. Probst [38], S. Pulvirenti [19], G. Quéméner [42], N. Randazzo [1], S. Razzaque [49], D. Real [4,*], S. Reck [38], G. Riccobene [19], A. Romanov [11,41], A. Rovelli [19], F. Salesa Greus [4,*], D.F.E. Samtleben [14,46], A. Sánchez Losa [34,4], M. Sanguineti [11,41], D. Santonocito [19], P. Sapienza [19], J. Schnabel [38], M.F. Schneider [38], J. Schumann [38],

* Corresponding authors.
real@ific.uv.es (D. Real), dacaldia@ific.uv.es (D. Calvo), sagreus@ific.uv.es (F. Salesa Greus), km3net-pc@km3net.de
[a] Deceased.
[b] Also at Dipartimento di Fisica, INFN Sezione di Padova and Università di Padova, I-35131, Padova, Italy.

https://doi.org/10.1016/j.nima.2022.167132
Received 24 January 2022; Received in revised form 2 June 2022; Accepted 5 June 2022
Available online 8 July 2022

H.M. Schutte [20], J. Seneca [14], I. Sgura [34], R. Shanidze [45], A. Sharma [50], A. Sinopoulou [10], B. Spisso [40,6], M. Spurio [16,17], D. Stavropoulos [10], S.M. Stellacci [40,6], M. Taiuti [11,41], Y. Tayalati [15], H. Thiersen [20], S. Tingay [35], S. Tsagkli [10], V. Tsourapis [10], E. Tzamariudaki [10], D. Tzanetatos [10], V. Van Elewyck [3,48], G. Vasileiadis [51], F. Versari [16,17], D. Vivolo [6,27], G. de Wasseige [3], J. Wilms [52], R. Wojaczyński [47], E. de Wolf [14,25], T. Yousfi [22], S. Zavatarelli [11], A. Zegarelli [28,8], D. Zito [19], J.D. Zornoza [4], J. Zúñiga [4], N. Zywucka [20]

[1] INFN, Sezione di Catania, Via Santa Sofia 64, Catania, 95123, Italy
[2] Université de Strasbourg, CNRS, IPHC UMR 7178, F-67000 Strasbourg, France
[3] Université de Paris, CNRS, Astroparticule et Cosmologie, F-75013 Paris, France
[4] IFIC - Instituto de Física Corpuscular (CSIC - Universitat de València), c/Catedrático José Beltrán, 2, 46980 Paterna, Valencia, Spain
[5] Aix Marseille Univ, CNRS/IN2P3, CPPM, Marseille, France
[6] INFN, Sezione di Napoli, Complesso Universitario di Monte S. Angelo, Via Cintia ed. G, Napoli, 80126, Italy
[7] Università di Napoli "Federico II", Dip. Scienze Fisiche "E. Pancini", Complesso Universitario di Monte S. Angelo, Via Cintia ed. G, Napoli, 80126, Italy
[8] INFN, Sezione di Roma, Piazzale Aldo Moro 2, Roma, 00185, Italy
[9] Universitat Politècnica de Catalunya, Laboratori d'Aplicacions Bioacústiques, Centre Tecnològic de Vilanova i la Geltrú, Avda. Rambla Exposició, s/n, Vilanova i la Geltrú, 08800, Spain
[10] NCSR Demokritos, Institute of Nuclear and Particle Physics, Ag. Paraskevi Attikis, Athens, 15310, Greece
[11] INFN, Sezione di Genova, Via Dodecaneso 33, Genova, 16146, Italy
[12] University of Granada, Department of Computer Architecture and Technology/CITIC, 18071 Granada, Spain
[13] Universitat Politècnica de València, Instituto de Investigación para la Gestión Integrada de las Zonas Costeras, C/ Paranimf, 1, Gandia, 46730, Spain
[14] Nikhef, National Institute for Subatomic Physics, PO Box 41882, Amsterdam, 1009 DB, Netherlands
[15] University Mohammed V in Rabat, Faculty of Sciences, 4 av. Ibn Battouta, B.P. 1014, R.P. 10000 Rabat, Morocco
[16] INFN, Sezione di Bologna, v.le C. Berti-Pichat, 6/2, Bologna, 40127, Italy
[17] Università di Bologna, Dipartimento di Fisica e Astronomia, v.le C. Berti-Pichat, 6/2, Bologna, 40127, Italy
[18] KVI-CART University of Groningen, Groningen, Netherlands
[19] INFN, Laboratori Nazionali del Sud, Via S. Sofia 62, Catania, 95123, Italy
[20] North-West University, Centre for Space Research, Private Bag X6001, Potchefstroom, 2520, South Africa
[21] Instituto Español de Oceanografía, Unidad Mixta IEO-UPV, C/ Paranimf, 1, Gandia, 46730, Spain
[22] University Mohammed I, Faculty of Sciences, BV Mohammed VI, B.P. 717, R.P. 60000 Oujda, Morocco
[23] Università di Salerno e INFN Gruppo Collegato di Salerno, Dipartimento di Matematica, Via Giovanni Paolo II 132, Fisciano, 84084, Italy
[24] ISS, Atomistilor 409, Măgurele, RO-077125, Romania
[25] University of Amsterdam, Institute of Physics/IHEF, PO Box 94216, Amsterdam, 1090 GE, Netherlands
[26] TNO, Technical Sciences, PO Box 155, Delft, 2600 AD, Netherlands
[27] Università degli Studi della Campania "Luigi Vanvitelli", Dipartimento di Matematica e Fisica, viale Lincoln 5, Caserta, 81100, Italy
[28] Università La Sapienza, Dipartimento di Fisica, Piazzale Aldo Moro 2, Roma, 00185, Italy
[29] Università di Bologna, Dipartimento di Ingegneria dell'Energia Elettrica e dell'Informazione "Guglielmo Marconi", Via dell'Università 50, Cesena, 47521, Italy
[30] Cadi Ayyad University, Physics Department, Faculty of Science Semlalia, Av. My Abdellah, P.O.B. 2390, Marrakech, 40000, Morocco
[31] University of the Witwatersrand, School of Physics, Private Bag 3, Johannesburg, Wits 2050, South Africa
[32] Università di Catania, Dipartimento di Fisica e Astronomia "Ettore Majorana", Via Santa Sofia 64, Catania, 95123, Italy
[33] INFN, LNF, Via Enrico Fermi, 40, Frascati, 00044, Italy
[34] INFN, Sezione di Bari, via Orabona, 4, Bari, 70125, Italy
[35] International Centre for Radio Astronomy Research, Curtin University, Bentley, WA 6102, Australia
[36] Subatech, IMT Atlantique, IN2P3-CNRS, Université de Nantes, 4 rue Alfred Kastler - La Chantrerie, Nantes, BP 20722 44307, France
[37] University Würzburg, Emil-Fischer-Straße 31, Würzburg, 97074, Germany
[38] Friedrich-Alexander-Universität Erlangen-Nürnberg, Erlangen Centre for Astroparticle Physics, Erwin-Rommel-Straße 1, 91058 Erlangen, Germany
[39] Western Sydney University, School of Computing, Engineering and Mathematics, Locked Bag 1797, Penrith, NSW 2751, Australia
[40] Università di Salerno e INFN Gruppo Collegato di Salerno, Dipartimento di Fisica, Via Giovanni Paolo II 132, Fisciano, 84084, Italy
[41] Università di Genova, Via Dodecaneso 33, Genova, 16146, Italy
[42] Normandie Univ, ENSICAEN, UNICAEN, CNRS/IN2P3, LPC Caen, LPCCAEN, 6 boulevard Maréchal Juin, Caen, 14050, France
[43] University of Granada, Dpto. de Física Teórica y del Cosmos & C.A.F.P.E., 18071 Granada, Spain
[44] NIOZ (Royal Netherlands Institute for Sea Research), PO Box 59, Den Burg, Texel, 1790 AB, Netherlands
[45] Tbilisi State University, Department of Physics, 3, Chavchavadze Ave., Tbilisi, 0179, Georgia
[46] Leiden University, Leiden Institute of Physics, PO Box 9504, Leiden, 2300 RA, Netherlands
[47] National Centre for Nuclear Research, 02-093 Warsaw, Poland
[48] Institut Universitaire de France, 1 rue Descartes, Paris, 75005, France
[49] University of Johannesburg, Department Physics, PO Box 524, Auckland Park, 2006, South Africa
[50] Università di Pisa, Dipartimento di Fisica, Largo Bruno Pontecorvo 3, Pisa, 56127, Italy
[51] Laboratoire Univers et Particules de Montpellier, Place Eugène Bataillon - CC 72, Montpellier Cédex 05, 34095, France
[52] Friedrich-Alexander-Universität Erlangen-Nürnberg, Remeis Sternwarte, Sternwartstraße 7, 96049 Bamberg, Germany
[53] Université de Haute Alsace, rue des Frères Lumière, 68093 Mulhouse Cedex, France
[54] University of Münster, Institut für Kernphysik, Wilhelm-Klemm-Str. 9, Münster, 48149, Germany
[55] Utrecht University, Department of Physics and Astronomy, PO Box 80000, Utrecht, 3508 TA, Netherlands
[56] INFN, CNAF, v.le C. Berti-Pichat, 6/2, Bologna, 40127, Italy

ARTICLE INFO

Keywords:
Time calibration
Instrumentation
Neutrino telescopes

ABSTRACT

The KM3NeT Collaboration is currently constructing a multi-site high-energy neutrino telescope in the Mediterranean Sea consisting of matrices of pressure-resistant glass spheres, each holding a set of 31 small-area photomultipliers. The main goals of the telescope are the observation of neutrino sources in the Universe and the measurement of the neutrino oscillation parameters with atmospheric neutrinos. A relative time synchronisation between photomultipliers of the nanosecond order needed to guarantee the required angular resolution of the detector. Due to the large detector volumes to be instrumented by KM3NeT, a cost reduction of the different systems is a priority. To this end, the inexpensive Nanobeacon has been designed and developed by the KM3NeT Collaboration to be used for detector time-calibration studies. At present, more than 600

Nanobeacons have been already produced. The characterisation of the optical pulse and the wavelength emission profile of the devices is critical for the time calibration. The optical pulse rise time has been quantified as less than 3 ns, while the Full Width Half Maximum is less than 6 ns. The wavelength drift, due to a variation of the supply voltage, has also been qualified as lower than 10 nm for the full range of the Nanobeacon. In this paper, more details about the main features of the Nanobeacon design, production and operation, together with the main properties of the light pulse generated are described.

1. Introduction

The KM3NeT Collaboration [1] is building a network of underwater neutrino telescopes at two deep locations in the Mediterranean Sea. Although the same technology is used for the two detectors their configuration is different, reflecting the difference in scientific goals. Astroparticle Research with Cosmics in the Abyss (ARCA [2]) has been designed for the detection of neutrinos of astrophysical origin with energies from ∼ 100 GeV to PeV, and is located 100 km off the southern tip of Sicily (Italy) at a depth of 3500 m. Oscillation Research with Cosmics in the Abyss (ORCA [3]), which mainly aims at studying the fundamental properties of neutrinos, is located 40 km south of the coast of Toulon (France) at a depth of about 2450 m. The detection principle is based on the collection of Cherenkov photons produced along the path of relativistic charged particles emerging from neutrino interactions inside or in the vicinity of the detector.

The telescopes are designed as 3-dimensional matrices of light detectors, spanning a large volume, as shown in Fig. 1. The active component is the Digital Optical Module (DOM) [4–6], a pressure-resistant glass sphere which houses 31 photomultipliers (PMTs). The arrival time of the Cherenkov photons, together with the position of the DOMs allow the reconstruction of the trajectory of the primary neutrino. The resolution of the reconstructed neutrino trajectory in the detector depends on the accurate measurement of the arrival time of the light on the optical sensors, with a precision better than one nanosecond, and of their position in space, better than 20 cm. A good timing calibration is therefore mandatory to ensure the reliability of the track reconstruction algorithms. The precision required for the relative time calibration system derives from the transit time spread (TTS) of the photomultipliers (σTTS ∼ 1.3 ns) and the effect of the chromatic dispersion in water (∼1.5 ns for a typical light path of 40 m). The addition in quadrature of these contributions leads to a best possible time resolution of ∼2 ns per single photon. The measurement of the detection times of the PMT hits is based on clock signals which are distributed from shore so that a common reference time is used in the whole apparatus, as explained in Section 3. The clock distribution system determines the propagation delays for these signals to reach the different electronics containers offshore with sub-nanosecond precision. The time measurements from individual PMTs have however to be corrected by appropriate offsets, which are determined in situ by means of a calibration system based on LED and laser devices (optical beacons) emitting light flashes at known times [7]. In order to ensure that the apparatus reaches its maximum pointing accuracy, it is necessary that the accuracy with which all such offsets are determined, in the so-called relative time calibration, remains below 1 ns, so that the resulting systematic error is significantly smaller than the intrinsic event-by-event fluctuations.

For that reason, time and position calibration of the telescope is a critical requirement. The main data acquisition electronic board of the DOM [8,9] is the Central Logic Board (CLB) [10,11], which performs the readout of the 31 PMT channels. A power board [12] mounted on top of the CLB provides power. The DOMs are distributed along lines, called Detection Units (DUs), each hosting 18 DOMs. In ORCA, the vertical spacing between DOMs is around 9 m, while in ARCA it is 36 m. The DUs are anchored on the seafloor, with a spacing about 20 m in ORCA, and 90 m in ARCA and are organised in Building Blocks (BB), each one composed of 115 DUs. The first fourteen DUs of KM3NeT, six for ORCA and eight for ARCA, have already been deployed and are currently taking data [13].

1.1. The Nanobeacon system

In addition to the information encoded in the clock distribution time using a customised version [14] of the White Rabbit protocol [15,16], there are several methods of *in-situ* time calibration. The key is redundancy, which allows for verifying other calibration systems, reducing any systematic error. In addition to down-going muons and photons from ^{40}K radioactive decays in the seawater, KM3NeT has an optical beacon system based on pulse generation devices. Two different sources of short-pulsed light [17] are used to cross-check the time calibration of the telescope by illuminating sets of the optical modules in a controlled scenario: the laser beacon [18], and the Nanobeacon [19], the latter being the subject of the present work. Both beacons complement each other, having the laser beacon more range and with good performance for inter-line calibration, especially in the lower storeys where the illumination redundancy is lower. It also can be used for positioning, while the Nanobeacon can add more redundancy with a lower cost.

Each DOM houses a Nanobeacon (Fig. 2). The Nanobeacon can produce a short-duration pulse approximately 5 ns wide (FWHM), with around 3 ns rise time (from 10% to 90% of full amplitude) and with enough intensity to illuminate the DOMs located on the same DU above the emitting DOM. With a good understanding of the optical pulse shape and control of the time of emission, the Nanobeacon pulses can be used to monitor the relative time offsets between DOMs of the same DU.

The intensity of the pulse and the viewing angle (defined as the solid angle of the cone containing 50% of the light emission) of the LED emission have also been proven relevant for the calibration between DUs, as a proper selection of these values allows the illumination of the neighbouring DUs with Nanobeacon flashes. The effect of high-intensity pulses has been studied in the past for the LED Optical Beacon of ANTARES [20]. In order to avoid this effect in KM3NeT, the Nanobeacon timing calibration will operate at single photoelectron level. The position of the Nanobeacon 45° off the axis from the top of the DOM is chosen to reduce the effect of sedimentation and biofouling on the glass sphere of the DOM. The Nanobeacon has its origin in the LED beacon system used for the time calibration of the Astronomy with a Neutrino Telescope and Abyss environmental RESearch (ANTARES) experiment [21]. ANTARES, which is still operational after more than 13 years in the Mediterranean Sea close to the ORCA site, is the predecessor of KM3NeT and is based on the same detection principle but with smaller instrumented volume. The ANTARES LED beacon consists of a glass and titanium container housing 36 LEDs with their corresponding electronic pulsers.

The electronics and the control firmware of the Nanobeacon are presented in Sections 2 and 3, respectively, while studies of the LED model are addressed in Section 4. The mass production of Nanobeacons for KM3NeT is described in Section 5, together with the test setup and the results of the intensity tests performed just after production. The proof of concept is illustrated in Section 6, while the characterisation of the optical pulse in terms of rise time and width are presented in Section 7. Moreover, the results of the pulse characterisation in terms of wavelength are discussed in this Section. Finally, in Section 8, a summary is presented together with future plans.

2. Nanobeacon electronics

The LED beacon has been considerably simplified in KM3NeT by integrating the LED inside the DOM. This avoids the need for a mechanical external container and significantly reduces the cost (around

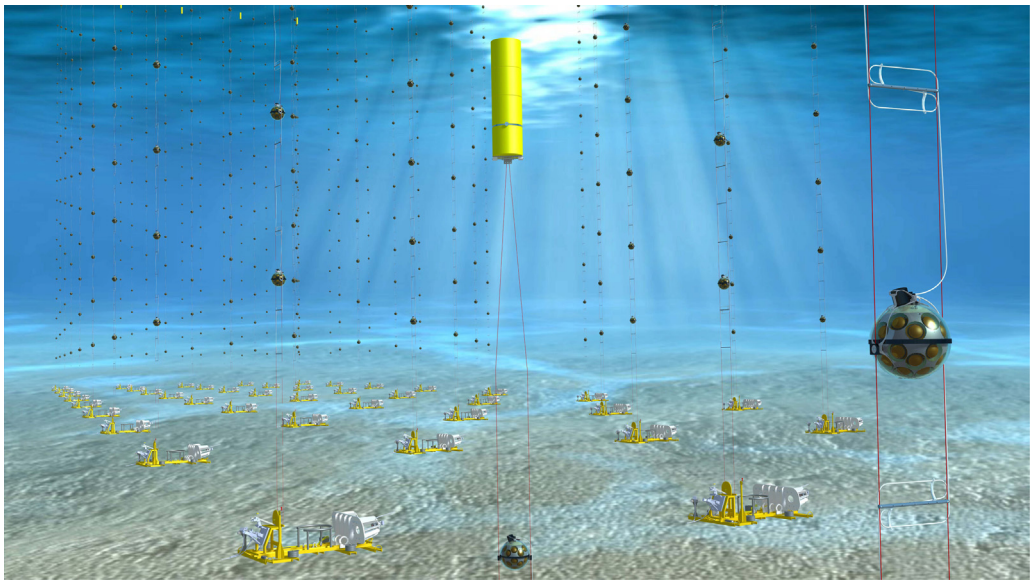

Fig. 1. Artistic view of KM3NeT. The illustration is not scaled: sunlight does not reach the depths at which the KM3NeT detector is deployed. The total volume of the detector, once completed, will be larger than one km^3.

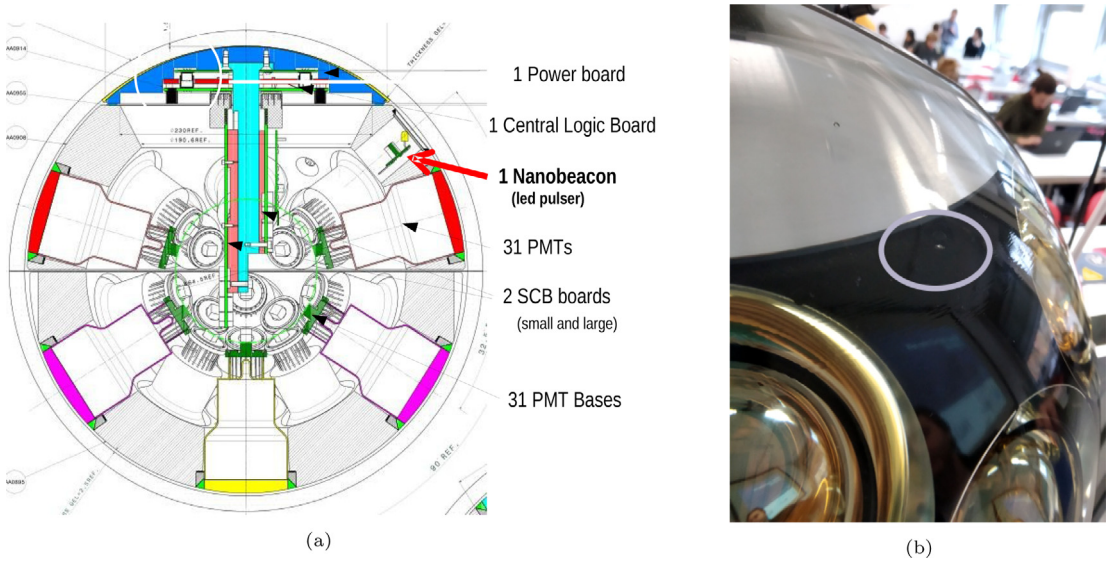

Fig. 2. (a) 2D sketch of the DOM, showing the position of the Nanobeacon LED at 45° from the vertical axis. The main components of the DOMs are shown: the PMTs, the cooling system and the main electronic boards. (b) A picture of a small part of the top hemisphere of the KM3NeT optical module with the aluminium cooling cap visible. The DOM sphere has a diameter of 17" (43 cm). The position of the Nanobeacon is highlighted by the circle.

50 €). The Nanobeacon is composed of two different elements: the pulser, and the DC/DC converter. The pulser comprises the LED and the electronics board that generates the trigger for the optical pulse. The DC/DC converter is integrated in the power board inside the DOM, which generates the power supply to the DOM, including the Nanobeacon pulser voltage. The power generated in the power board is fed to the Nanobeacon via the CLB. The control of the Nanobeacon voltage and the generation of the electrical trigger are both carried out at the CLB.

2.1. Nanobeacon pulser

The Nanobeacon pulser is based on the Kapustinsky circuit [22], which can generate short pulses with simple electronics, modified for KM3NeT. The main modification allows for the use of a positive trigger signal. The schematics of the pulser are shown in Fig. 3. The trigger of the pulser is generated by an FPGA on the CLB, which provides a 1.5 V negative square pulse. The pulse generated is added to the DC voltage provided by the power supply rail. The DC voltage loads a capacitor (C2) that is discharged to the LED during the transition of two transistors (Q1 and Q2) working in opposition. The switching between transistors is triggered by the signal provided by the FPGA, provoking the discharge of the capacitor to the LED and the emission of a narrow optical pulse. The trigger generated by the FPGA is provided to the Nanobeacon pulser by a three-wire twisted cable to reduce the electromagnetic induced noise. This connection also provides ground and power, which comes from the power board.

2.2. Nanobeacon power supply

The Nanobeacon control voltage is provided by one of the rails of the power board, which converts the 12 V input into the voltage needed to operate the Nanobeacon. The power rail consists of a DC/DC converter working in a buck-boost configuration, providing a voltage

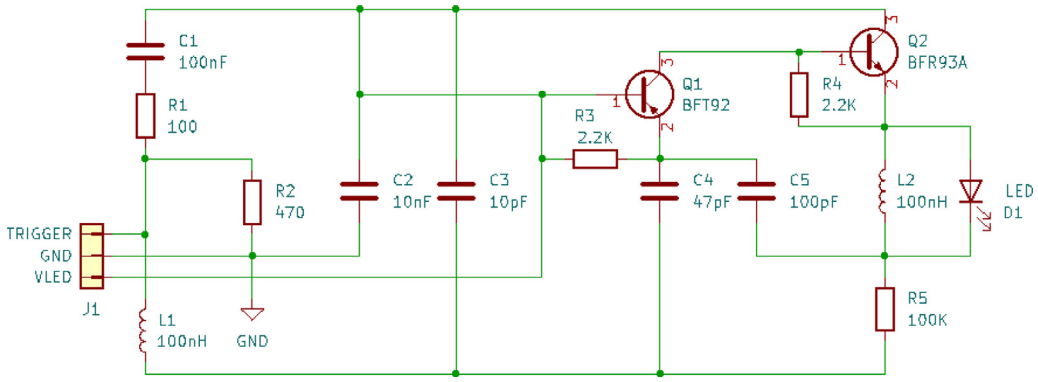

Fig. 3. Electronics schematics of the Nanobeacon pulser.

configurable between 4.5 and 30 V, via a 10-bit DAC controllable by I^2C. When the output voltage of the DAC changes, the voltage of the Nanobeacon power supply is modified accordingly. The provided voltage determines the amount of current supplied to the LED, and therefore, the intensity of the generated optical pulse. The DC voltage charges the capacitor while the trigger performs a fast discharge through the LED. The coil in parallel develops charge in opposition to the discharging capacitor reducing its time constant. The power supply includes two circuits for measuring the voltage and the current. The values provided by these circuits are acquired with an ADC that is read by the FPGA embedded software. As will be shown in Section 7, the voltage is correlated with the pulse width: the lower the voltage supplied, the narrower the optical pulse. The typical power consumption of the Nanobeacon does not exceed 0.1 W.

3. Firmware

An Intellectual Property (IP) block, implemented in the CLB FPGA, generates the trigger signal for the Nanobeacon. This FPGA IP core implements a Wishbone slave [23], where 5 registers of 32 bits are accessible via the embedded software to configure the Nanobeacon trigger signal (Table 1). In particular, the first register allows for enabling and disabling the trigger signal. For this, one of the bits of the first register, called *Enable control*, is used. Another bit, called *Enable power*, controls the power supply of the Nanobeacon. There are, therefore, two different methods for enabling the Nanobeacon, being the power supply the first step in KM3NeT, followed by the logic enabling of the Nanobeacon. In KM3NeT, the data acquisition is organised in *timeslices*, which have a typical duration of 100 ms. The start of the timeslices is synchronous with the CLB 62.5 MHz White Rabbit clock. A second register (m1) allows for defining the delay of the first flash after the start of the timeslices. A third register (m2) defines the Nanobeacon pulse length. The flash period is configured in a fourth register (m3), and the number of triggers per timeslice is defined in the fifth one (m4). In all cases, the time is coded in ticks of 16 ns (the period of the 62.5 MHz clock). Table 1 describes the different control registers that configure the IP core to trigger the Nanobeacon pulse. The operation of the Nanobeacon firmware is illustrated in Fig. 4. The configuration of the last 4 registers defines the characteristics of the flash rate, while the control of the pulse is implemented in the first register. Before starting the LED flashing, an I^2C command is sent via embedded software to the Nanobeacon rail to set the voltage. In addition to the configuration, the IP core sends an interrupt to the embedded software after the end of each flashing pattern in a timeslice has ended, giving feedback of the operation performed.

4. Comparison of the LED model candidates

Several LED models (AVAGO HLMP-CB26, AVAGO HLMP-CB30, AGILENT HLMP-AB87, and Nichia NSPB500S) were tested in the laboratory and *in situ* in one of the ANTARES lines. The viewing angle of the models analysed ranges from 10° to 30°. The light intensity is one order of magnitude higher than the intensity of the LED model used in ANTARES, where the top part of the LEDs used was cleaved. The results of the tests performed using the ANTARES line are shown in Fig. 5. Each point represents the average number of hits per flash detected on a storey, which in the case of the ANTARES test were spaced by approximately 15 m. The results are presented for all LED models under study and compared to the original ANTARES LED beacon. The target storey situated at 150 m from the emitting beacon detects approximately 0.1 hit per flash emitted by the ANTARES LED beacon, while other LED models considered for KM3NeT record values ranging from 0.4 to 1.05 hits per flash. The angular distribution of the analysed LED models is wide enough to perform intraline calibration, i.e., to illuminate the DOMs of the same DU. The angular aperture is important to maximise the number of DOM illuminated by a single Nanobeacon. The first KM3NeT tests have shown that it is also possible to illuminate the DOMs of the nearest DUs, even in the case of ARCA where the lines are spaced 90 m away. The final LED model chosen for KM3NeT is the HLMP-CB1A-XY0DD by Broadcom. This model is the recommended replacement of the two LEDs from Avago (CB26 and CB30) tested on the ANTARES line, which were obsolete and not available at the moment of the final decision as Broadcom acquired Avago. The main characteristics of this LED are summarised in Table 2 together with the rest of LED analysed and the minimum criteria to be fulfilled in terms of FWHM, viewing angle, wavelength and luminous intensity.

According to the manufacturer, the viewing angle of the chosen LED model is 15° in air. However, the angular aperture is modified by the light transitions through materials with different refraction indices, such as the DOM glass sphere and the seawater. The LED is held vertically by a mechanical structure with the LED top close to the borosilicate glass of the DOM sphere (refractive index 1.47 while the seawater refractive index is estimated in 1.38). An original viewing angle of 15° in air has been calculated to increase to 76.5° once in seawater. In order to measure the real viewing angle, a light-tight water tank available at the Laboratoire AstroParticule & Cosmologie, Paris, France (APC) was used. A DOM equipped with an embedded Nanobeacon was immersed in the water tank as shown in Fig. 6. The inner walls of the tank were painted in black to minimise reflections. The DOM was mounted in a mechanical structure allowing its rotation. During the test, the water tank was completely closed and darkened. The sensor used is a PD300-UV from Ophir, with a spectral range of 200–100 nm, a power range of 20 pW–300 mW, and a response time of 0.2 s. It was installed in three different positions of the water tank: two were located on one corner of the water tank, about 10 cm below the tank cover and right above the water surface. One of them was facing down while the other one was facing sideways. The third position was at the top cover of the tank, over the vertical axis of the DOM and 10 cm over the water surface. This distance was kept at the minimum value to minimise reflections and refraction at the water/air boundary. The three sensor positions were recording the measured light intensity

Table 1
Control registers of the Nanobeacon IP core. The first register includes the two control enabling/disabling bits, while the remaining registers parameterise the pattern of the Nanobeacon trigger.

Reg	Name	Remark
0 × 00	Enable register	Bit 0:Enable control - Bit 1:Enable power - Bits(2-31):Not used
0 × 01	Delay after TimeSlice	In 16 ns ticks (default 0 ns)
0 × 02	Nanobeacon Pulse Width	In 16 ns ticks (default 64 ns)
0 × 03	Nanobeacon Pulse Period	In 16 ns ticks (default 50 μs)
0 × 04	Number of pulses	Number of pulses per timeslice (default 100 pulses)

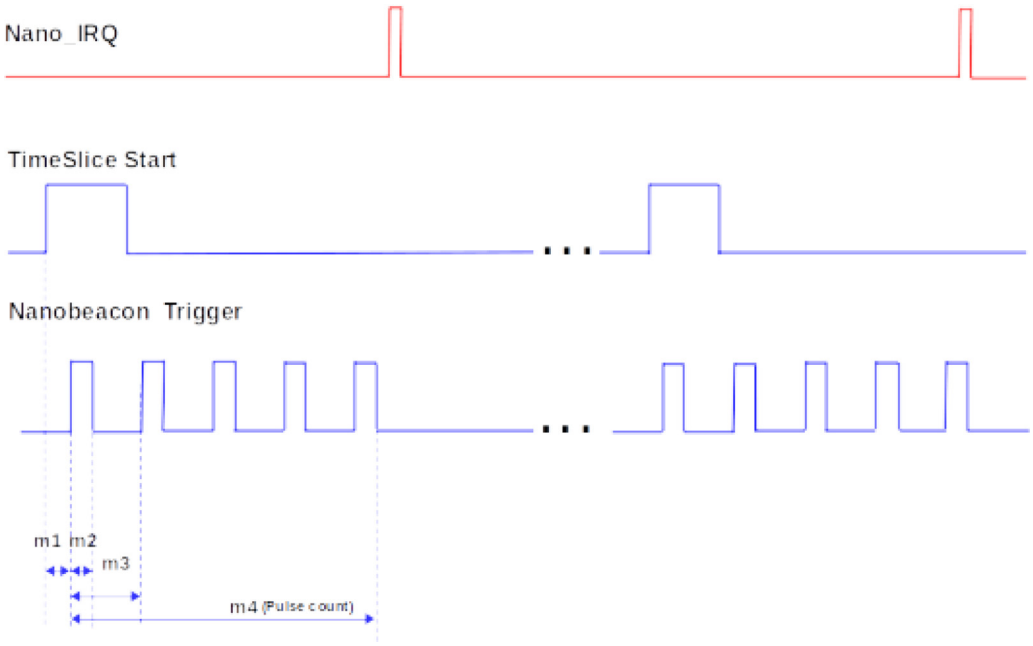

Fig. 4. Scheme of the Nanobeacon firmware IP core operation. The Nanobeacon trigger is defined by the delay after the start of the timeslice (m1, coded in the second register), the number of pulses per timeslice (m4, coded in the fifth register), the duty cycle of the pulse (m2, coded in the third register) and its period between pulses (m3, coded in the fourth register). The interrupt (Nano_IRQ) generated by the firmware IP core when the number of pulses per timeslice has ended is also shown.

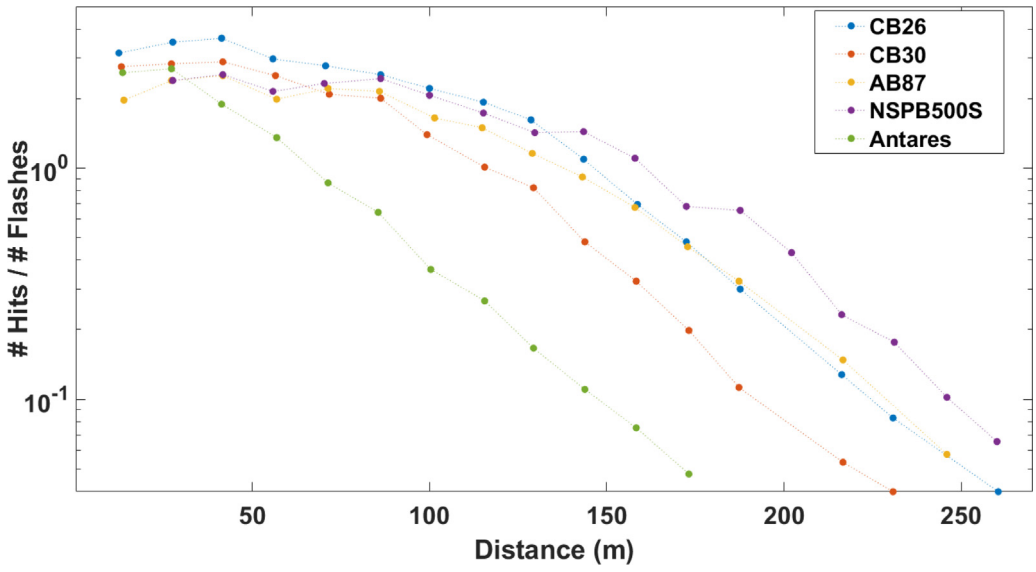

Fig. 5. Results of the *in-situ* tests in one of the ANTARES lines of the preselected KM3NeT LEDs. The average number of hits recorded in each storey per flash is shown as a function of the distance from the flashing LED. Each point represents one storey, the stories are spaced 15 m apart. The final selected LED model for KM3NeT (HLMP-CB1A-XY0DD) is the recommended replacement of CB26 and CB30, which was tested to check that their main characteristics were compliant to KM3NeT requirements. The targets in KM3NeT have been established at least 150 metres with a minimum required of 0.1 hits/flash.

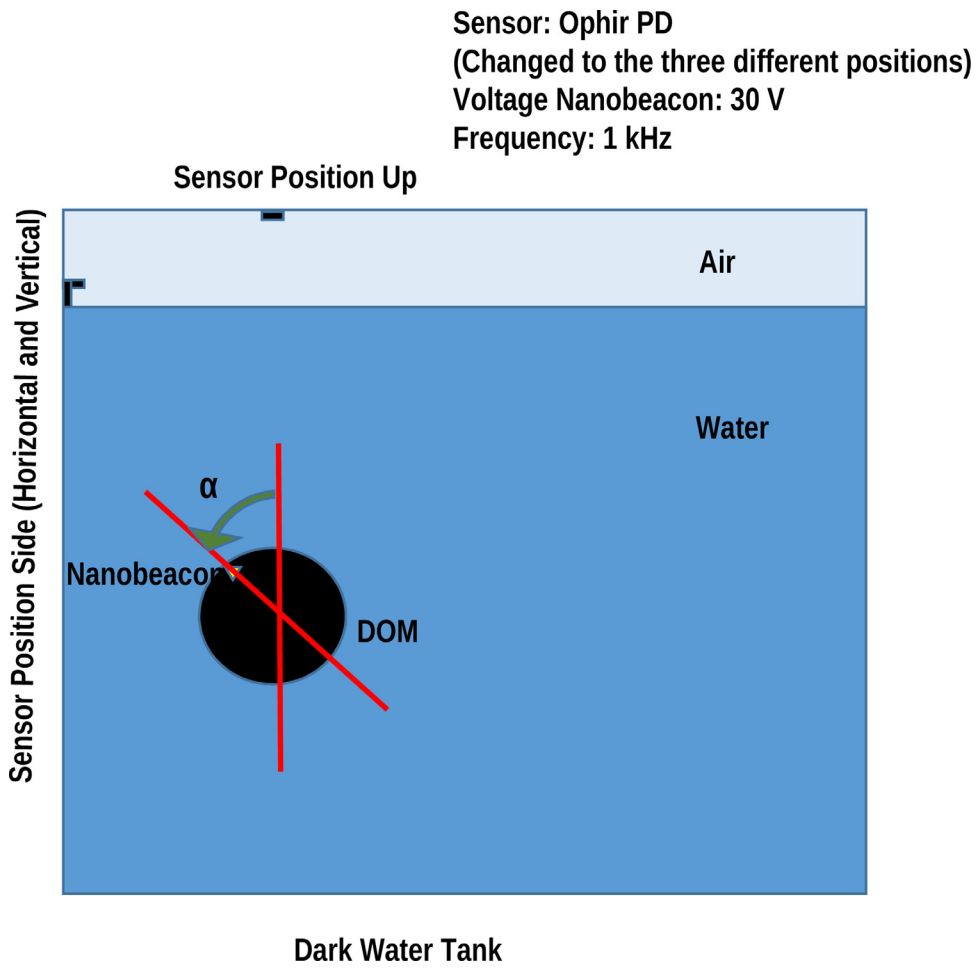

Fig. 6. Light-tight water tank setup. A DOM is submerged in the tank at a depth of approximately 2 m. The DOM can rotate, as shown in the figure. A light sensor is moved to three different positions on the upper part of the container, collecting the light emitted by the Nanobeacon being flashed in the DOM.

Table 2
Main characteristics of the selected LED (HLMP-CB1A-XY0DD) and the tested LED models in ANTARES. All the models are build in a package T-1 3/4 of 5 mm, except the AB87, which is 5 mm Mini Oval. The asymmetric emission of this LED model has been the main reason of its disqualification in KM3NeT.

Attribute	CB1A	NSPB500S	AB87	CB26	CB30	Criteria
Wavelength (nm)	470	453	464	466	470	> 450
Viewing Angle (deg)	15	19	50	23	28	> 10
Luminous intensity (pJ)	150	170	130	150	90	> 80
FWHM (ns)	4.6	6.1	4.6	4.6	4.3	< 6.0

while the DOM with the flashing LED was being rotated. Fig. 7 shows the data read out for different angle positions. The data have been normalised to the maximum value. The angular aperture of the selected LED model in water exceeds 40°, much larger than the nominal value in air, and compatible with the calculated data.

5. Manufacturing and tests

The first prototypes of the Nanobeacon, eight in total, were installed on the Neutrino Mediterranean Observatory (NEMO) Phase II prototype tower [24], and three more were integrated on the prototype DU of KM3NeT [25]. Since then, 600 Nanobeacon boards have been produced for KM3NeT, of which at present more than 200 are in operation in the deep sea. All Nanobeacons incorporate the same LED model, the HLMP-CB1A-XY0DD. The company in charge of the production also performed a calibration test, measuring the light emission intensity at different voltages. This is necessary since there is a noticeable difference in the light intensity between LEDs. The setup used by the company included a mechanical framework composed of two PVC pieces manufactured at the IFIC (Instituto de Física Corpuscular, Valencia, Spain) workshop. The mechanical framework fixes the Nanobeacon to one of the PVC pieces while it encloses the Nanobeacon in complete darkness with the other piece. This upper piece, which has a little hole to allow the light exit from the Nanobeacon, has a space reserved to hold the head (818-UV) of the Newport energy meter 1835-C. The test setup is shown in Fig. 8. The light intensity has been measured at 10 V, 16 V, 20 V, and 24 V. The measured values of the mean light intensity at each voltage are stored in the database of KM3NeT for later use. The mean values and the standard deviation of the 600 measurements are presented in Table 3; the standard deviation values indicate significant intrinsic variations in intensity among individual LEDs. The standard deviation of the measurements performed with this testsetup is lower than 1%

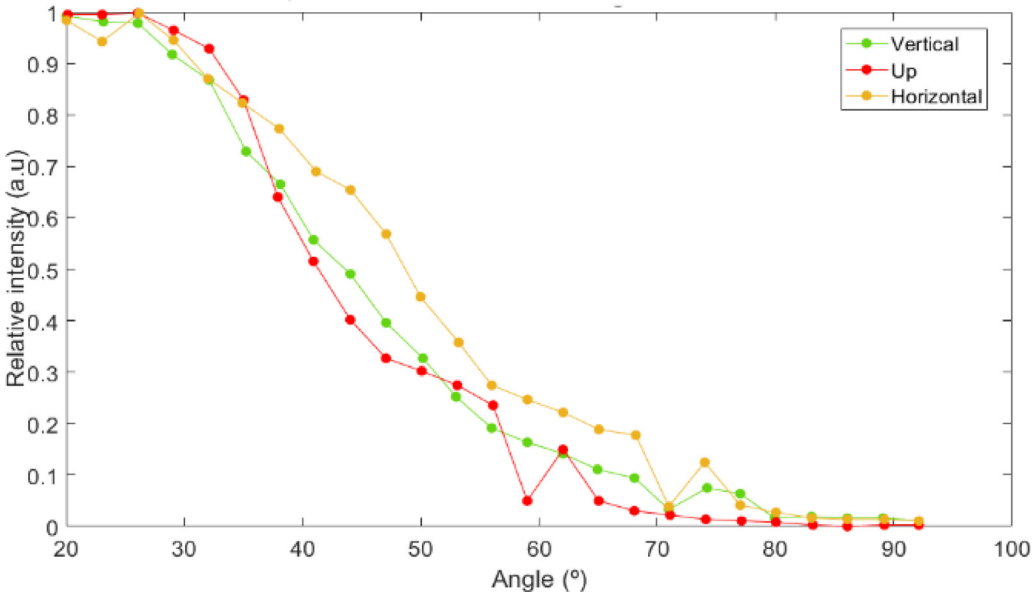

Fig. 7. Light intensity as a function of the polar angle measured in the water tank setup in three different positions. Data have been normalised to the maximum light intensity. The x-axis does not start at zero because there were mechanical limitations in the rotation mechanism of the DOM. Also negative values could not be reached. The instrumental error of the 1%, the points are of that order.

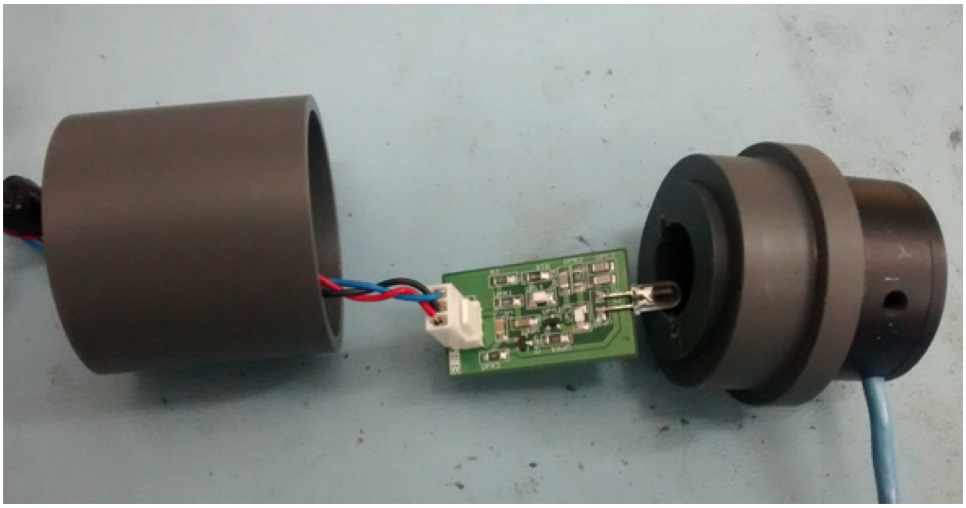

Fig. 8. Setup used for the production tests. Note the Nanobeacon between the two PVC pieces and the head of the intensity meter coupled with the PVC piece on the right.

5.1. Nanobeacon reliability

Nanobeacons are expected to remain operative on a regular basis for at least 20 years, with a variable frequency depending on the calibration needs. Currently, Nanobeacon operation is performed weekly in KM3NeT with a flashing frequency of 10 kHz and a typical duration of 10 min. In order to qualify its reliability, a FIDES[a] analysis has been applied to the Nanobeacon board as to most of the KM3NeT electronics boards [26]. The resulting FIT[b] value is 10, which is a very low value thanks to the simplicity and robustness of the Nanobeacon electronics, corresponding to a life expectancy longer than 20 years. Moreover, the Nanobeacon will be working only during dedicated calibration runs, which represent a small fraction of the detector lifetime. In addition, since every DOM includes a Nanobeacon, a high level of redundancy is assured as a single Nanobeacon is able to illuminate several nearby DOMs.

Table 3
Results of the intensity test performed after the first batch of the Nanobeacon production. The table presents the mean and the standard deviation of the intensity measurements performed on the 600 produced Nanobeacons showing the variations from Nanobeacon to Nanobeacon in the optical energy when supplied with the same voltage. Note the large values of the standard deviations. The error of the setup is lower than 1%.

Voltage (V)	10	16	20	24
Mean intensity (nW)	2.3	22.2	49.7	85.3
Standard deviation (nW)	3.8	18.8	30.3	41.7

6. Proof of concept

The time calibration potential of the Nanobeacon in terms of volume coverage and redundancy is demonstrated in Fig. 9. Data from

[a] FIDES means "faith" in Latin. It is the name chosen by the methodology for components reliability developed under the supervision of DGA (French MoD)

[b] FIT stands for *Failure in Time* and indicates the number of failures per 10^9 operation hours.

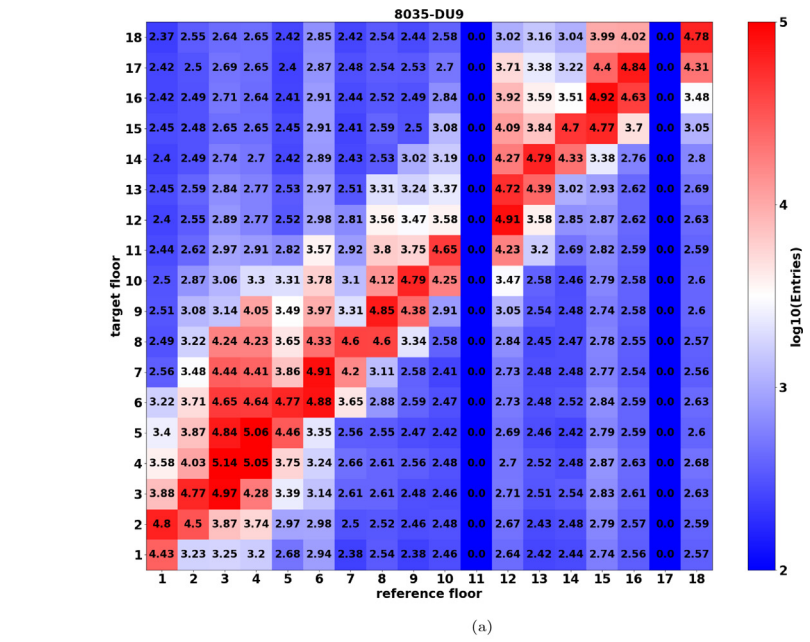

(a)

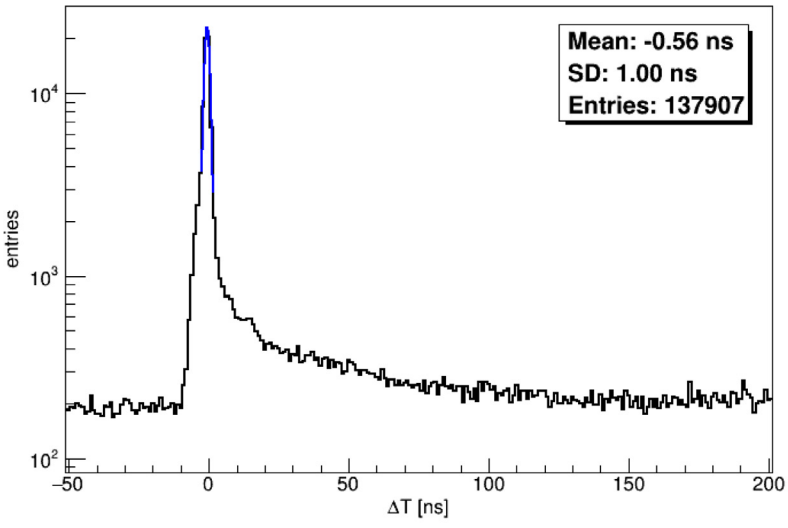

(b)

Fig. 9. (a) Schematic view of the result of a Nanobeacon calibration run in KM3NeT. The x-axis shows the reference storey, i.e., the position of the light-emitting DOM in the DU (1 closest to the see storey, 18 on top); the y-axis the target storey, i.e., the position of the light-receiving DOM in the DU. The Nanobeacons were flashed sequentially with a delay of 3520 ns between one storey and the following. All Nanobeacons were set to a default voltage (8 V). The plot shows that a total coverage of the detector can be achieved with high redundancy. Therefore, the Nanobeacons have the ability of monitoring the time offsets of the PMTs in the same DOM, and in different DOMs in the same DU. For this particular run the DOMs at storey 11 and 17 were not operative. The source of prepulses are K40 hits. (b) Time difference between the signal received in the target DOM (second storey) and light emission in the reference DOM (first storey), corrected for the light propagation time in seawater. The time difference between the reference and the destination is corrected by all offsets, even by the light propagation time. The peak obtained should be centre at zero, so the deviation is the value of the temporal calibration. It is always possible to illuminate a DOM flashing the DOM immediately below, but as there is so much redundancy the idea is to create a matrix and resolve it. This should give measurements of the calibration precision. The number of entries reduces the weight.

a calibration run taken in May 2020 have been used, with all the Nanobeacons in the line flashed sequentially with an operating voltage of 8 V. It is shown it is possible to illuminate the complete line with high redundancy. It can be seen that with two dead DOMs it is possible to calibrate the storey immediately above them (hits are detected in those DOMs when the DOM below the damage DOM is flashed. From the number of entries in the plot one can deduce that the intensities provided by the Nanobeacon differ by a factor 3, demonstrating the importance of individually calibrating the Nanobeacons before the deployment. Note that in the future the Nanobeacons will be operating with an individually calibrated V, providing all of them with almost equal intensities. The flashing frequency was 1 kHz. For flashing in the order of the kHz and even for the floor at higher distance, and with runs of a couple of minutes enough statistics will be achieved an relative error lower than 5%.

7. Optical pulse characteristics

The rise time and width of the optical pulse shape and the spectrum of the emitted light must be characterised in order to evaluate their effect on the time calibration. In this section, the results of the qualification are presented, together with a brief description of the methods used.

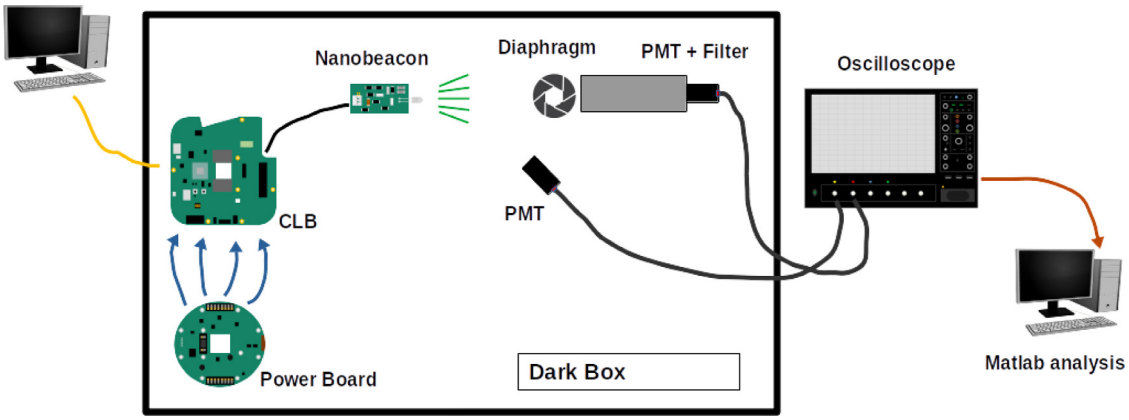

Fig. 10. Testbench for the measurement of the optical pulse. Inside a dark box, a Nanobeacon controlled by a CLB is flashed. Two PMTs are used. One PMT (a Hamamatsu H653 PMT with a transit time spread lower than 200 ps) includes a filter and a diaphragm in order to attenuate the signal to a level corresponding to one single photo electron (SPE). Then, the other PMT, (a Hamamatsu H6780-03 PMT with a photo-cathode of 8 mm diameter, a rise time of 0.8 ns and a transit time of 5.4 ns) receives the pulse directly to be used as time reference. The output of both PMTs is conducted to one digital oscilloscope where the skew between both signals is measured.

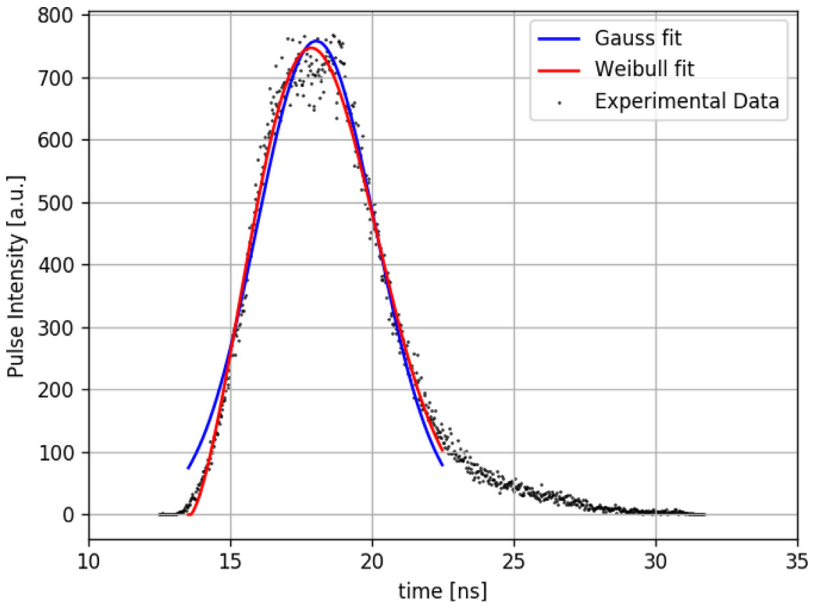

Fig. 11. Optical pulse shape obtained with the SPE method fitted with the Gaussian and Weibull functions. Note that the Weibull function fits the experimental data better, especially at the rise time region. The zero corresponds to the events where the two PMT fall times occur at the same time. For a given set of models, the one that describes the data better is the one that minimises the AIC [27], in this case the Weibull fit.

7.1. Pulse shape

7.1.1. Single photoelectron method

The SPE technique [28] has been chosen to measure the rise time and the width of the Nanobeacon emitted pulse. Fig. 10 shows the scheme of the measurement setup. The technique allows for the reconstruction of the pulse shape independently of the gain and rise time of the detector. A light sensor, usually a PMT with a low transit time spread (TTS) and enough sensitivity to detect single photons, is needed. In this case, two detectors have been used in the experimental setup: a Hamamatsu H6780-03 PMT with a photo-cathode of 8 mm diameter, a rise time of 0.8 ns and a transit time of 5.4 ns is used as trigger and provides an electrical signal generated by the first photons arriving from the optical pulse. A second detector, a Hamamatsu H653 PMT with a transit time spread lower than 200 ps and high sensitivity, measures the arrival time of the photons in the attenuated pulse. The jitter between the electrical trigger and the signal of trigger PMT has been measured in advance and it is of 140 ps. The jitter between two H6780 has been measured to be of only 15 ps. The Nanobeacon pulse is attenuated by means of optical filters so that only one or no photoelectron per pulse reaches the PMT. To ensure the PMT only detects single photon hits, a level of filtering that triggers no more than one over 100 Nanobeacon pulses is set. In this way, the probability to have no signal at all is 99%. Assuming Poissonian statistics, it is straightforward to estimate that the average number of single photoelectrons per flash is lower than $\mu = 0.01$, and the probability to have two single photoelectrons in the same flash is negligible (0.005%).

The signals of both PMTs are measured by a digital oscilloscope with a high bandwidth and sampling period. The time differences between the trigger and the SPE PMT are measured and accumulated in a histogram that reproduces the optical pulse shape and allows the measurement of the rise time (10%–90%) and the FWHM of the pulse. The time of each PMT is given by the 50% level of the falling edge, obtaining the time offset by subtracting both times. The distribution of the time differences reproduces the optical shape because the probability that a single photon arrives at the SPE PMT is related to the shape of the optical pulse, i.e., photons in the centre of the optical pulse have higher probability to be detected than those in the leading or trailing region of the optical pulse. This technique has numerous advantages with respect to the use of PMTs of high precision. First of all, the SPE technique is

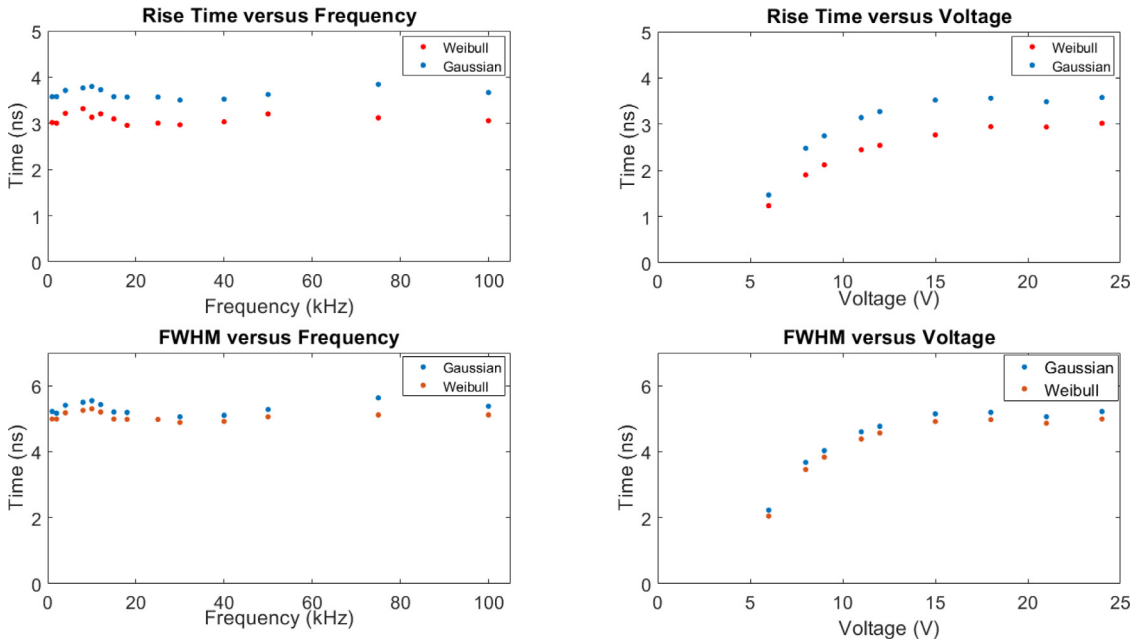

Fig. 12. Rise time and width (FWHM), obtained from Gaussian and Weibull fits, as a function of flashing frequency and applied voltage. When varying the frequency the voltage is fixed at 24 V. When varying the voltage the frequency is fixed at 1 kHz. Note the correlation of the voltage with the pulse width. The error is of the order of the marker.

Table 4
Mean values of the rise time and the FWHM for a Gaussian and a Weibull fit. The results for 24 LEDs of the model HLMP-CB1A-XY0DD being powered at 24 V and triggered at 1 kHz are presented.

N LEDs	Rise time (ns)		FWHM (ns)	
	Gaussian	Weibull	Gaussian	Weibull
Mean value	3.14	2.69	4.39	4.51
Standard deviation	0.27 (8.6%)	0.21 (7.8%)	0.38 (8.6%)	0.41 (9.1%)

based on the measurement of the temporal differences of two signals, greatly reducing the residual errors. Moreover, the digitisation of the signals is very effective and has higher time resolution if a digital oscilloscope with high bandwidth, sampling period and large memory is used. Large memory is specially useful in order to acquire the sufficient number of hits and increase the precision of the measurement. Finally, high precision PMTs are considerably more expensive than the PMTs needed to perform the SPE technique.

7.1.2. Results

In order to measure the rise time and the width of the optical pulse produced by the LED model chosen for KM3NeT, the pulse shape of 24 LEDs was measured using the SPE technique. The pulse shape was measured for each LED using a voltage of 24 V and a frequency of 1 kHz. The time distribution obtained for one of the LEDs using the SPE technique is shown in Fig. 11. The results of the fits to Gaussian and Weibull functions are superimposed. In Table 4 the mean and the standard deviation of the rise time and the width (FWHM) of the 24 LEDs using a Gaussian and a Weibull function is shown. The rise time and the FWHM of the optical pulses are about 2.69 and 4.51 ns respectively, with a statistical accuracy around 8%–9%. From the figure, it can be appreciated that the Weibull function matches the data better, in particular at the beginning of the pulse, providing a more precise description of the rise time of the pulse.

7.1.3. Effect of voltage and flashing frequency on the pulse shape

Rise time and FWHM of the optical pulse have been measured at different voltages and frequencies in order to evaluate the impact of these two parameters in the shape of the optical pulse. Each set of LED data has been fitted using a Weibull and a Gaussian function. The voltages have been varied between 6 V and 24 V, while maintaining a fixed frequency of 1 kHz. In another set of tests, the frequency has been varied from 1 kHz up to 100 kHz keeping the voltage fixed at 24 V. All the tests have been carried out using the same test equipment (Electronics + Nanobeacon + LED). As can be seen in Fig. 12, the impact of the frequency on the rise time and the FWHM of the optical pulse is negligible, and the fluctuations are compatible with the measurement uncertainties. However, the voltage has a clear impact on both rise time and FWHM. At low voltages (6 V), both decrease to levels only half of the values measured at higher voltages. The lower the voltage, the fainter and narrower the optical pulse, giving lower values of rise time and FWHM. This is especially true for voltages below 15 V. Note that the minimum rise time of 1.24 ns (Weibull fit) at 6 V is very close to the rise time of the electrical trigger signal. The mean of the rise time of the electrical trigger signal, after 1100 electrical pulses have been measured, has been computed to be 1.34 ns with a standard deviation of 50 ps.

7.2. Wavelength characteristics

The wavelength spectrum of the optical pulse is of great importance as the water optical properties depend on the wavelength, therefore it has an impact on the travel time of the pulse and in the time calibration. The wavelength spectrum of the optical pulse was measured for a set of 8 LEDs with an imaging spectrometer (Triax 190 de Horiba Scientific) at different voltages. The LEDs were tested at 30 V, 24 V, 20 V, 18 V, 15 V, 14 V and 13 V, keeping the frequency fixed at 1 kHz. Changes in the frequency do not affect the wavelength distribution. The spectral wavelength of an LED is shown in Fig. 13, where a Gaussian and a Weibull fit are superimposed. The wavelength spectra for different voltage values are shown in Fig. 14. The wavelength spectrum distribution shape does not change, but the wavelength peak slightly moves towards lower values when the voltage increases. This can also be seen graphically in Fig. 15. The shift in the wavelength is a well-known effect caused by the forward intensity, which is driven by the voltage applied. On average, the distribution shifts 2 nm to higher wavelength values when the voltage decreases by 5 V, this change being larger for lower

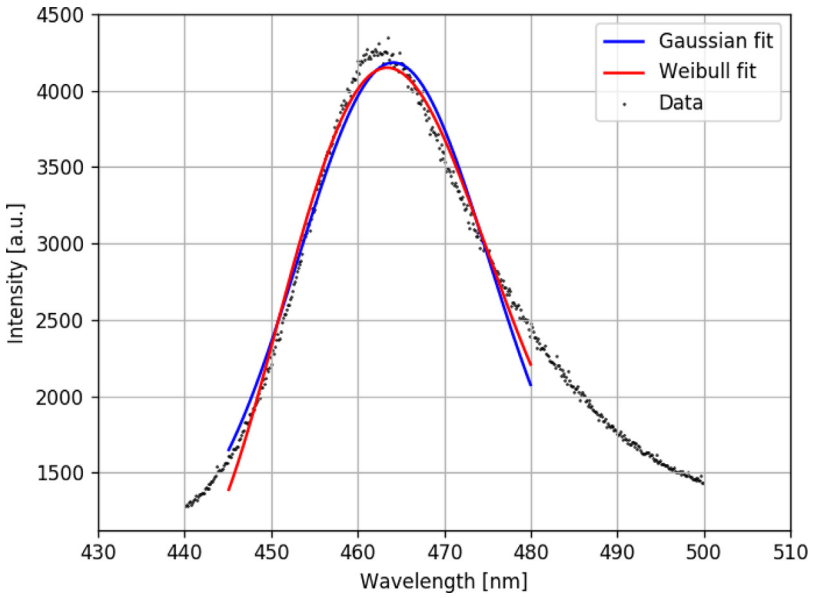

Fig. 13. Wavelength spectrum of an LED operated at 30 V and 1 kHz. Both, a Gaussian and a Weibull fit are included. In this case the Weibull fit minimises the AIC.

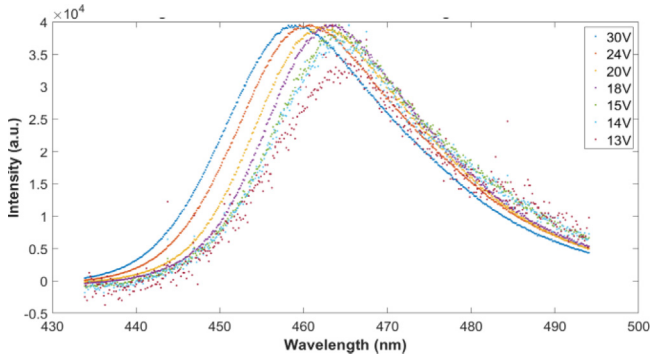

Fig. 14. Wavelength spectra for different voltage values. The data are normalised to the maximum intensity. The wavelength distribution shifts to higher wavelengths when the voltage is reduced.

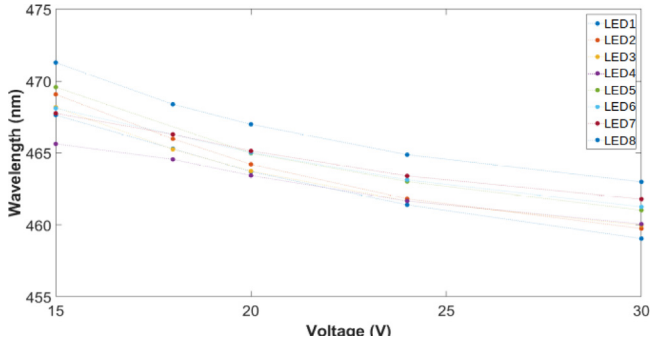

Fig. 15. Change of the central wavelength, calculated with the Weibull fit, as a function of the voltage applied for a sample of 8 LEDs. The central wavelengths vary slightly with the voltage, increasing as the voltage decreases. The error is of the order of the marker.

voltages. A variation of 10 nm in the light wavelength corresponds to a change in the refraction index lower than 0.06% [29]. The impact of this effect will not prevent the use of the Nanobeacon as a time accurate (one ns resolution) source over pathlengths higher than 100 m.

8. Summary

In order to ensure the high angular resolution required for the reconstruction of the neutrino direction in KM3NeT, a relative time synchronisation of the order of 1 ns between DOMs is needed. Different time calibration systems have been developed to this end. One of them is the Nanobeacon device which is presented in this article. The time properties of the basic electronics together with the firmware used for the operation of the board are described. The properties (rise time and width) of the optical pulse generated by the Nanobeacon have been evaluated, taking into account the impact of voltage and frequency on its performance. The wavelength spectrum of the optical pulses has also been measured, as well as the effect of the input voltage. The results obtained show that the Nanobeacon is an excellent instrument with low cost. The characterisation performed, measuring the optical pulse and its wavelength distribution, will be of great help during KM3NeT operation. The future plans include the analysis of LED models with different wavelength (ranging from near ultraviolet to green) and higher intensity that could be deployed in KM3NeT for water properties characterisation.

Declaration of competing interest

The authors declare that they have no known competing financial interests or personal relationships that could have appeared to influence the work reported in this paper.

Data availability

Data will be made available on request.

Acknowledgements

The authors acknowledge the financial support of the funding agencies: Agence Nationale de la Recherche (contract ANR-15-CE31-0020), Centre National de la Recherche Scientifique (CNRS), Commission Européenne (FEDER fund and Marie Curie Program), Institut Universitaire de France (IUF), LabEx UnivEarthS (ANR-10-LABX-0023 and ANR-18-IDEX-0001), Paris Île-de-France Region, France; Shota Rustaveli National Science Foundation of Georgia (SRNSFG, FR-18-1268),

Georgia; Deutsche Forschungsgemeinschaft (DFG), Germany; The General Secretariat of Research and Technology (GSRT), Greece; Istituto Nazionale di Fisica Nucleare (INFN), Ministero dell'Università e della Ricerca (MIUR), PRIN 2017 program (Grant NAT-NET 2017W4HA7S) Italy; Ministry of Higher Education Scientific Research and Professional Training, ICTP through Grant AF-13, Morocco; Nederlandse organisatie voor Wetenschappelijk Onderzoek (NWO), the Netherlands; The National Science Centre, Poland (2015/18/E/ST2/00758); National Authority for Scientific Research (ANCS), Romania; Ministerio de Ciencia, Innovación, Investigación y Universidades (MCIU): Programa Estatal de Generación de Conocimiento (refs. PGC2018-096663-B-C41, -A-C42, -B-C43, -B-C44) (MCIU/FEDER), Generalitat Valenciana: Prometeo (PROMETEO/2020/019), Grisolía (ref. GRISOLIA/2018/119) and GenT (refs. CIDEGENT/2018/034, /2019/043, /2020/049) programs, Junta de Andalucía (ref. A-FQM-053-UGR18), La Caixa Foundation (ref. LCF/BQ/IN17/11620019), EU: MSC program (ref. 101025085), Spain.

References

[1] S. Adrián-Martínez, et al., KM3NeT Collaboration, Letter of intent for KM3NeT 2.0, J. Phys. G 43 (8) (2016) 084001, http://dx.doi.org/10.1088/0954-3899/43/8/084001, 373.
[2] R. Coniglione, KM3NeT-ARCA project status and plan, EPJ Web Conf. 116 (2016) 11003, http://dx.doi.org/10.1051/epjconf/201611611003.
[3] J. Brunner, KM3NeT - ORCA: Measuring neutrino oscillations and the mass hierarchy in the Mediterranean Sea, in: PoS ICRC2015, 2016, p. 1140, http://dx.doi.org/10.22323/1.236.1140.
[4] S. Adrian-Martinez, et al., Deep sea tests of a prototype of the KM3NeT digital optical module (KM3NeT Coll.), Eur. Phys. J. C 74 (2014) 3056, http://dx.doi.org/10.1140/epjc/s10052-014-3056-3.
[5] E. Leonora, et al., KM3NeT Collaboration, Design and production of the digital optical module of the KM3NeT project, EPJ Web Conf. 136 (2017) 4008, http://dx.doi.org/10.1051/epjconf/201712604008.
[6] S. Adrián-Martínez, et al., KM3NeT Collaboration, Deep sea tests of a prototype of the KM3NeT digital optical module, Eur. Phys. J. C 74 (2014) 3056, http://dx.doi.org/10.1140/epjc/s10052-014-3056-3.
[7] J.A. Aguilar, et al., ANTARES Collaboration, Time calibration of the ANTARES neutrino telescope, Astropart. Phys. 34 (7) (2011) 539–549, http://dx.doi.org/10.1016/j.astropartphys.2010.12.004; Nucl. Instrum. Methods Phys. Res. A 578 (2007) 498-509, http://dx.doi.org/10.1016/j.nima.2007.05.325.
[8] D. Real, D. Calvo, Digital optical module electronics of KM3NeT, Phys. Part. Nuclei 47 (2016) 918–925, http://dx.doi.org/10.1134/S1063779616060216.
[9] S. Aiello, et al., KM3NeT Collaboration, KM3NeT digital optical module electronics: Hardware, firmware and software, J. Astron. Telesc. Instrum. Syst. 5 (4) (2019) 046001, http://dx.doi.org/10.1117/1.JATIS.5.4.046001.
[10] D. Calvo, D. Real, Status of the central logic board (CLB) of the KM3NeT neutrino telescope, J. Instrum. 10 (2015) C12027.
[11] D. Real, et al., KM3NeT acquisition: The new version of the central logic board and its related power board, with highlights and evolution of the control unit, J. Instrum. 15 (2020) C03024.
[12] A. Belias, Design and development of the power supply board within the digital optical module in KM3NeT, in: PoS TIPP 2014, 2014, p. 188, Proceeding to the 3th TIPP, Amsterdam, 2014.
[13] M. Ageron, et al., KM3NeT Collaboration, Dependence of atmospheric muon flux on seawater depth measured with the first KM3NeT detection units, J. Eur. Phys. C 80 (2020) 99, http://dx.doi.org/10.1140/epjc/s10052-020-7629-z.
[14] R. Coniglione, et al., KM3NeT Collaboration, KM3NeT time calibration, in: Proceeding to ICRC, 2019.
[15] J. Serrano, et al., The white rabbit project, in: Proc. 12th Int. Conf. on Accelerator and Large Experimental PhysicsControl Systems, ICALEPCS'09, Kobe, Japan, Oct. 2009, Paper TUC004, pp. 93–95.
[16] M. Lipinskis, et al., White rabbit: A PTP application for robust sub-nanosecond synchronization, in: 2011 IEEE International Symposium on Precision Clock Synchronization for Measurement, Control and Communication, 2011, pp. 25–30, http://dx.doi.org/10.1109/ISPCS.2011.6070148.
[17] D. Real, D. Calvo, KM3NeT Collaboration, The time calibration system of KM3net: The laser beacon and the nanobeacon, Ad-hoc networks and wireless, in: ADHOC-NOW 2014, in: Lecture Notes in Computer Science, vol. 8629, Springer, Berlin, Heidelberg, 2015.
[18] D. Real, KM3NeT Collaboration, Proposal of a new generation of laser beacon for time calibration in the KM3NeT neutrino telescope, AIP Conf. Proc. 1630 (2014) 130, http://dx.doi.org/10.1063/1.4902789.
[19] D. Calvo, KM3NeT Collaboration, Nanobeacon: A low cost time calibration instrument for the KM3NeT neutrino telescope, AIP Conf. Proc. 1630 (2014) 138, http://dx.doi.org/10.1063/1.4902791.
[20] J.A. Aguilar, Analysis of the Optical Beacon System and Search for Point-Like Sources in the ANTARES Neutrino Telescope (Ph.D. thesis), 2007.
[21] M. Ageron, et al., ANTARES Collaboration, The antares optical beacon system, Nuclear Instrum. Methods Phys. Res. A 578 (2007) 498–509, http://dx.doi.org/10.1016/j.nima.2007.05.325.
[22] J.S. Kapustinsky, et al., A fast timing light pulser for scintillation detectors, Nucl. Instrum. Methods Phys. Res. A 241 (1985) 612.
[23] R. Herveille, WISHBONE system-on-chip (SoC) interconnection architecture for portable IP cores, specifications, 2002.
[24] Adrián-Martínez, et al., Long term monitoring of the optical background in the Capo Passero deep-sea site with the NEMO tower prototype, Eur. Phys. J. C 76 (2016) 68, http://dx.doi.org/10.1140/epjc/s10052-016-3908-0.
[25] Adrián-Martínez, et al., The prototype detection unit of the KM3NeT detector, Eur. Phys. J. C 76 (2016) 54, http://dx.doi.org/10.1140/epjc/s10052-015-3868-9.
[26] D. Real, et al., Reliability studies for KM3NeT electronics: The FIDES method, in: Proceeding to ICRC, Busan, 2017.
[27] H. Akaike, A new look at the statistical model identification, IEEE Trans. Automat. Control 19 (6) (1974) 716–723, http://dx.doi.org/10.1109/TAC.1974.1100705.
[28] J.E. McMillan, The Single Photon Technique for Measuring LED Pulser Flash Width, Sheffield Particle Astrophysics, Sheffield University – Department of Physics and Astronomy Internal Publication, 1999, SH-HEP-99-07.
[29] C. Parrish, Index of refraction of seawater and freshwater as a function of wavelength and temperature, 2020, http://research.engr.oregonstate.edu/parrish/index-refraction-seawater-and-freshwater-function-wavelength-and-temperature. Consulted the 29th May 2021.

Diego Real is a Ph.D. in Physics and Research Engineer at Instituto de Física Corpuscular. He received his B.S. in Electronics in 1997 and his M.S. in Control and Electronics in 2000, both from the Polytechnic University of Valencia. He is the author of several publications on electronics. His Ph.D. was awarded by Spanish Astronomy Academy with the Prize in the Instrumentation Category. His current research interests include acquisition and synchronisation systems for particle physics. He is, since 2013, the Electronics project leader of the KM3NeT telescope and member of the Technical Advisory Board of the GVD-Baikal telescope.

David Calvo is a Ph.D. in Physics and research engineer at Instituto de Física Corpuscular of Valencia. He received his M.S. in Computing in 2006 from University Jaume I, his M.S. in Electronics in 2009 from University of Valencia and his M.S. in electronic systems design in 2012 from the Polytechnic University of Valencia. His research interests are focused on the digital electronics, synchronisation and readout acquisition systems. He is the author of several publications on electronics.

Francisco Salesa is a Distinguished Researcher at Institut de Física Corpuscular (IFIC) since 2019. He received his Physics Degree from University of Valencia in 2003, his master degree in 2006, and his Ph.D. in Physics in 2010 with the title "Time Calibration and Point Source Analysis with the ANTARES Neutrino Telescope", work which was awarded in 2012 with the "Premi Extraordinari de Doctorat" for outstanding theses. He had several post-doctoral positions at Colorado State University (US) 2011–2013, Penn State University (US) 2013–2015, and Institute of Nuclear Physics (Poland) 2015–2019. He has worked for The Pierre Auger and The HAWC Gamma-ray Observatories, where he was in charge of the calibration of the detector. He is the author of several publications on detector calibrations. His research interests include multi-messenger astronomy and the search for sources of high-energy cosmic rays.